Proceedings of the
Annual Stability Conference
Structural Stability Research Council
Louisville, Kentucky, April 13-16, 2021

Effects of local buckling on the behavior of high-strength steel beams

Abdullah M. Alghossoon[1], Amit H. Varma[2]

Abstract
This paper focuses on the behavior, modeling, and evaluation of high-strength steel beams used as girders in composite moment resisting frame system MRFs. This research has led to the development and calibration of effective (phenomenological) stress-strain curves and fiber-based finite element approaches for modeling the behavior of high-strength steel beams. The key parameters influencing the cyclic behavior of high-strength steel beams are: (i) shape / geometric details, (ii) flange and web slenderness ratios, (iii) material stress-strain behavior, and (iv) fracture/Damage failure criteria. This paper summarizes the experimental data on the cyclic behavior of high-strength steel beams and develops 3D finite element models to model their behavior. The models are developed cognizant of the parameters (i) – (iv) listed above. The models are validated against experimental data and then used to conduct parametric studies to investigate the effects of material and geometric parameters on the cyclic behavior and ductility of high-strength steel beams. The developed effective stress-strain relationships hold the key to developing potential design methods based on allowable strain criteria and/or continuous strength methods recently developed by other researchers.

1. Introduction

The recent developments in the steel manufacturing industry have led to higher strength steels' production with enhanced properties such as material strength, toughness, and ductility. The availability of such higher strength steels has inspired engineers to consider them for optimizing member sizes in complex and demanding situations, particularly when seismic, fire or multiple hazards are being considered for the design basis. The increasing desire for adopting high-strength steel in buildings is driven by economical aspects such as maximizing the buildings' floor area and its revenue accordingly, as well as the implementation of high-strength steel in excess of 145 ksi in many buildings around the worlds. A recent report by the AISC committee has concluded that steel manufacturers are able to provide high-strength structural steel to the US market, but they currently do not see high and sustainable demand (AISC Committee on Specifications and Steel, 2019). From a structural perspective, the use of high-strength steel girders allows for lighter self-

[1] Ph.D. student, Purdue University, <aalghoss@purdue.edu>
[2] Professor, Purdue University, <ahvarma@purdue.edu>

weight sections, which leads to a more economical seismic design. Moreover, it allows for larger spans in the building, which distributes the building weights more towards the building's perimeter, hence; increasing its stability against overturning.

Recent research has evaluated the behavior of rectangular filled-composite members made from high-strength materials. These researches have led to the development and calibration of effective (phenomenological) stress-strain curves and fiber-based finite element approaches for modeling the behavior of high-strength composite columns. When used in special moment resisting frames (S-MRFs) for seismic design, the corresponding girders can also be made from high-strength steel to match the high strength of the composite columns.

Many researchers and engineers believe that it is time for the high strength materials in structures based on their promising performance in the filled-composite members and the composite moment-resisting frame system C-MRFs in construction. The match of the high strength concrete-filled tube columns CFT and the corresponding high strength steel girders is considered a candidate for higher performance composite moment-resisting frames in construction. The main hinder to using high-strength steel girders is the different properties the new steel material has compared with the conventional steels such as (ASTM A36, ASTM A572, ASTM A992, etc.) and the limited experimental and numerical studies are available in the literature investigating the cyclic behavior of high strength steel girder.

2. Background

The development of steel in the field of construction has taken its path at a slow pace compared to other fields such as automobiles and aviation, which are leading the research on material science in general to meet their continuous requirements. Dual-phase (PD), complex-phase (CP), and transformation-induced plasticity (TRIP) are examples of the advanced high strength steel (AHSS) types produced with yield strength higher than that permitted by the steel design codes meanwhile possessing other important properties such as ductility, weldability, and fracture toughness, (Shome and Tumuluru, 2015). Keeler et al. (2017) have reported many of the available advanced high-strength steel (AHSS), which has a tensile strength in excess of 1000 MPa (referred to as GigaPascal steel) and elongation comparable to that of mild steel.

The research on high-strength steel in construction has mainly focused on investigating its ductility. The investigation of the inelastic cyclic behavior of steel members is important to evaluate the system performance under extreme loading conditions such as earthquake loading. The AISC 360-16 requires a minimum rotational capacity R=3 in Eq.1 for the development of the full plastic flexural strength, a higher value of R is required for the seismic application. The limitation on the flange and web compactness shown in Eq.2 and Eq.3 in the AISC 360-16 design code was placed to ensure the development of the required rotational ductility.

$$R = (\theta_u / \theta_p - 1) \quad (1)$$

$$\lambda_{pf} = \frac{b}{2t_f} \leq 0.38\sqrt{\frac{E}{F_y}} \quad (2)$$

$$\lambda_{pw} = \frac{h}{t_w} \leq 3.76\sqrt{\frac{E}{F_y}} \quad (3)$$

The main concern about the performance of high-strength steel has always been its rotational ductility. Green (2000) has done extensive studies to quantify the structural ductility of high-strength steel members in his Ph.D. dissertation and his subsequent publications. He has examined the effects of material stress-strain characteristics, cross-sectional geometry, and various loading conditions through a series of tests on welded I-shaped HSLA-80 flexural members. His experimental results indicate that the stress-strain characteristics of HPS have a major influence on the inelastic behavior of flexural members compared to similar members made from mild steel, which means different compactness criteria have to be developed (Green et al., 2001).

Another experimental study by Schillo and Feldmann (2017) conducted on a high-strength steel beam shows that the rotation capacity R=3 was achieved by all the specimens made from S700 steel but not for the S970. They have also reported the influence of the loading condition by demonstrating more rotational capacity in the four-point loading beam than the three-point loading where strains are very localized.

Few attempts have been made to investigate the two-way cyclic behavior of the high-strength steel beam. Shinohara et al. (2012) have tested high-strength steel for H-shaped beams with a large depth-thickness ratio in the elastic and plastic range by conducting loading tests on a cantilever steel beam made of over 100 ksi yield stress. They have reached the same conclusion from the previous studies on a high-strength steel beam, which states that the current limit of compactness cannot be used for high-strength steel beams. Accordingly, they have proposed a new limit value of the plate slenderness ratio. They have also demonstrated that these beams are useful as seismic design beams.

A comprehensive investigation of high-strength steel members' behavior requires a benchmarked numerical model alongside the experimental investigations. It is well-known that local steel buckling and low-cycle fatigue can remarkably change the structure's cyclic response and must be considered in the numerical model. A recent study by Hai et al. (2019) developed a numerical model considering cyclic deterioration in strength and stiffness of high-strength steel beam-column for Q690 steel. According to their parametric analysis results, the level of axial loading, flange slenderness, web slenderness and loading amplitude are proportional to the cyclic deterioration in high-strength steel beam-column. Besides, the local-buckling-driven mode has a higher impact on cyclic degradation compared with the low-cycle-fatigue-driven mode.

Recently, there is an increasing trend towards developing a finite element fiber-based model or hysteretic model for high strength steel beam to ease the use of computer-aided static and dynamic analysis or conducting parametric studies. Wang et al. (2014) have investigated the seismic behavior of high-strength welded beam-column members. They have developed a trilinear hysteretic model for the end moment-rotation hysteretic curves to achieve more accurate descriptions of the cyclic performance of HSS specimens. The literature lacks an effective stress-strain curve for high-strength steel members that implicitly accounts for the local buckling, cyclic degradation, and fracture. This study is a continuation of other work by bridging the gap in high-strength steel members' fiber-based model.

3. Numerical Model

Model Description

The numerical analysis of the high-strength steel beam in this paper was conducted by calibrating a 3D finite element model using (ABAQUS-FEA/CAE 2019) based on experimental tests performed in prior research such as Shinohara et al. (2012) and Hai et al. (2019). The 3D finite element model was developed to account for several aspects that are believed to control the high-strength steel beam's cyclic behavior, such as the initial imperfection, residual stresses, material hardening model, and material damage model. The 3D beam model shown in Fig. 1 uses a second-order solid element C3D20R with an approximate size of 10 mm x 10 mm. the beam's boundary conditions are fixed at one end and free at the other end. The motion of the nodes at both surfaces was controlled using the kinematic coupling constraint option. The details of the model's main features, such as material calibration, initial imperfection, and residual stresses, are discussed in the next sections.

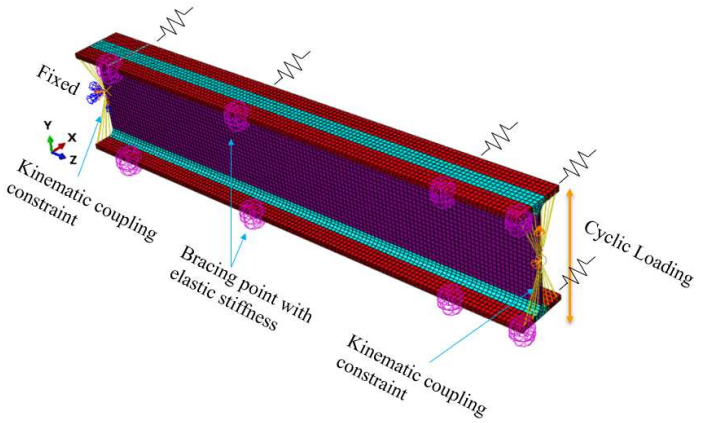

Figure 1: 3D finite element model in ABAQUS

Material model

The lab report of a steel coupon test demonstrates the steel's engineering stress-strain curve, while the stress-strain data input in the finite element software such as ABAQUS requires the true stress-strain since the elements' deformation can take place during analysis. The shape of the engineering stress-strain curve varies for different high-strength steel types but more comparable in the space of true stress-strain, as shown in Fig.2 by Keeler and Kimchi (2017) for DP steel type. The conversion between the engineering and the true stress-strain curve is quite simple based on the logarithmic Eq.4 and Eq.5. The drawback of the conversion equations is that it only works up to the necking point, where the reduction of the cross-section area equals the material strain hardening as in Eq.6. The state of stress beyond necking can no longer be considered uniaxial, and a different approach has to be considered to describe the material degradation. The deterioration of the system's hysteretic behavior is an accumulation of the strength and stiffness degradation on the material level of the finite elements.

$$\varepsilon_t = ln(1+\varepsilon_e) \quad (4)$$

$$\sigma_t = \sigma_e(1+\varepsilon_e) \quad (5)$$

$$d\sigma / d\varepsilon = \sigma \quad (6)$$

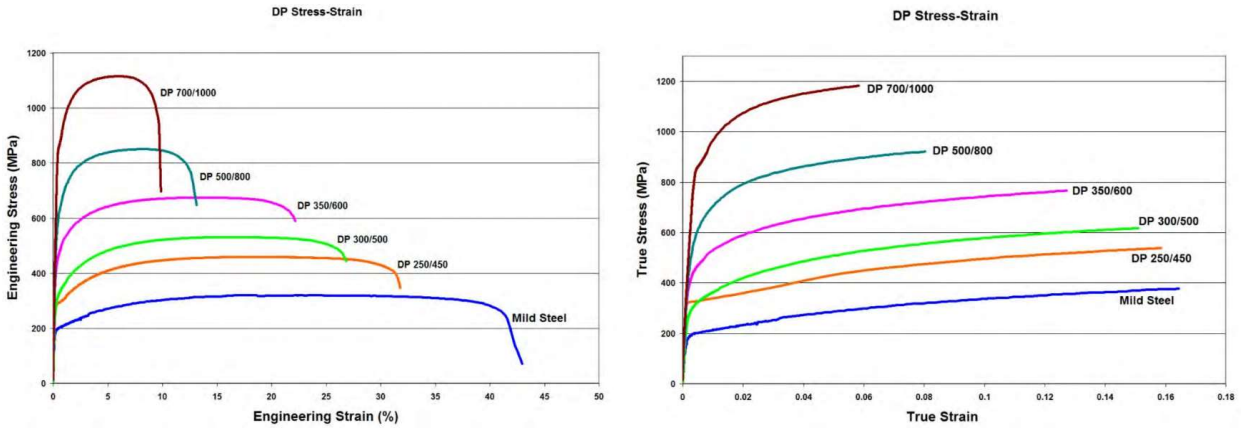

(a) (b)

Figure 2: Stress-strain curve for DP steel grade (Keeler and Kimchi, 2017): (a) Engineering SS curve. (b) True SS curve

The Engineering stress-strain curve from the coupon test by Shinohara et al. (2012) in Fig.3 (a) is adopted for the study model calibration. The digitalized version of this curve and the corresponding True stress-strain curve of the undamaged material are determined using the previous equations. The elastic behavior was characterized by the modulus of elasticity $E=29000\ ksi$ and the yield stress $F_y=115\ ksi$. The plastic behavior of the high-strength steel follows the nonlinear isotropic

/kinematic hardening model. This model is the most accurate in ABAQUS for the low-rate cyclic behavior of metal as it accounts for the reduction of the yield stress in one direction (Bauschinger effect and anisotropy) when straining in the opposite one. ABAQUS offers different ways to define the isotropic and kinematic parameters, such as tabular form or specifying the model parameters directly. In the case of limited test data, the first half cycle of a unidirectional tension test can be used to determine the required isotropic and kinematic parameters. The number of back stress was selected to be equal to the number of data points.

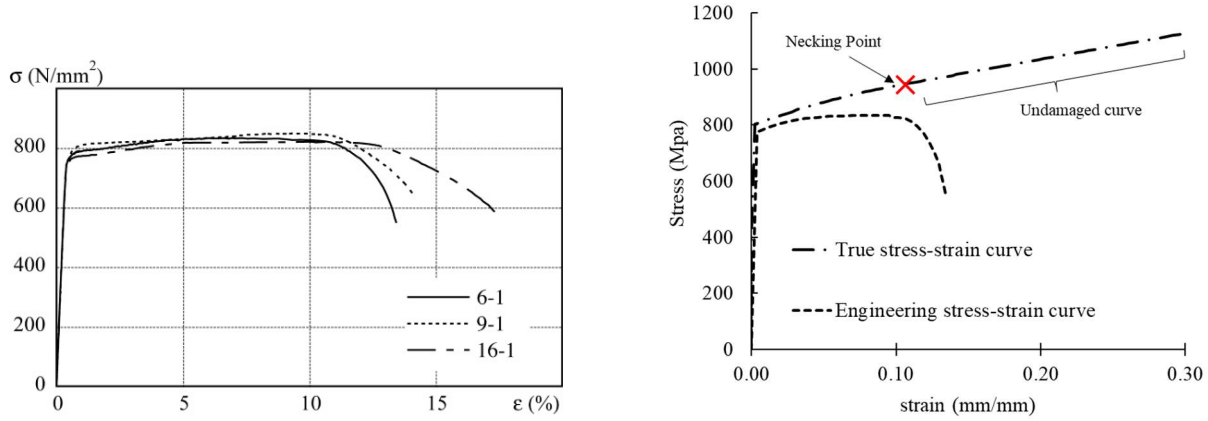

(a) (b)

Figure 3: (a) Stress-strain relationship by Shinohara et al. (2012), (b) Engineering and True stress-strain curve

Material damage model

Several approaches have been used to predict the ductile fracture of metal, such as the traditional fracture mechanics based on the existing crack assumptions and the continuum damage mechanics (CDM), which predicts the crack initiation of uncracked objects based on ductility criteria. The CDM has the advantage of familiarity and suitability for large-scale structural engineering applications. The ductility criterion in the CDM approach assumes that cracks first initiate when void nucleation occurs around the secondary particles (impurities) of metal and growing based on the state of the strain rate change. Finally, the neighbor voids open on each other to form a crack. This assumption requires understanding how the voids are growing and what is the critical size that would initiate damage. Rice and Tracey (1969) proposed a relationship between spherical void growth rate (dR / R_o) and stress triaxiality (T) as shown in Eq. 7 but without identifying the critical size criteria. The integration of Eq.7 leads to the relationship between the equivalent plastic strain at fracture (ε_{eqf}) and the stress triaxiality, as shown in Eq.8 and Eq.9. In order to account for the variation of the stress triaxiality during loading history, the incremental damage dD is calculated at each step (assuming constant triaxiality within the same step) of the analysis based on Miner's rule in Eq.10. The accumulated damage is then superimposed linearly till $D = 1$ which is the point of fracture. The element deletion will take effect during analysis when the damage index D reaches

its maximum value (default is 0.99). The evolution of the damage (starting from D=0 to D=1) has to be described in terms of the effective plastic displacement rather than strain. The latter idea is important to avoid the mesh-dependence caused by strain localization in softening models. The material damage evolution in this study was based on a linear stress-displacement response up to the point of failure. Eq. 12 demonstrates the equivalent plastic strain at fracture in uniaxial loading conditions (ε_{eqf}^{o}).

$$\frac{dR}{R_o} = 0.283\, e^{(1.5)T} d\varepsilon_{eq} \tag{7}$$

$$ln\left(\frac{R}{R_o}\right) = 0.283 \int_0^{\varepsilon_{eq}} e^{(1.5)T} d\varepsilon_{eq} \tag{8}$$

$$\varepsilon_{eqf} = ln\left(\frac{R_f}{R_o}\right) / 0.283\, e^{(1.5)T} = \mu_c\, e^{(-1.5)T} \tag{9}$$

$$\sum_{i=1}^{m} \frac{n_i}{N_i} = 1 \tag{10}$$

$$dD = \frac{d\varepsilon_{eq}^{p}}{\varepsilon^{p}(T)} \tag{11}$$

$$\varepsilon_{eqf}^{o} = \mu_c\, e^{-1.5/3} \tag{12}$$

Coupon test

The determination of the equivalent plastic strain at fracture requires conducting experimental and numerical simulations. The results of the high-strength steel coupon tests conducted by Shinohara et al. (2012) were adopted in this paper as shown in Fig.3. the numerical model of the coupon test shown in Fig. 4 follows the recommended specimen's dimension in the (ASTM E8, 2010). The Explicit analysis in ABAQUS was adopted for the coupon test simulation as it fits the highly non-linear static and quasi-static problems. The reduced integration C3D8 element was assigned the undamaged true stress-strain curve shown in Fig. 3 based on the modified weighted average model (MWA) proposed by Jia and Kuwamura (2014) in Eq.13, where $w = 1$ and necking point is determined based on Eq.6.

$$\sigma = \sigma_{necking} + w\sigma_{necking}(\varepsilon - \varepsilon_{necking}) \tag{13}$$

The determination of the damage initiation point in the load-displacement curve is a bit controversial. In this paper, damage initiates at the necking point, calculated as described previously. At this point, the equivalent plastic strain is found to be 12.5%, corresponding to stress triaxiality T_o = 1/3 for pure uniaxial tension (coupon test). Alternatively, this value can be calculated by measuring the reduction of cross-section area $A_R = (A_o - A_f)$ at the necking point and applying Eq. 14.

The damage evolution was calibrated to match the load-displacement curve of the coupon test, and the equivalent plastic strain at failure (ε^u_{eqf}) is found to be 112.5% for thin plates (<10mm) and 127.5% for thick plates. The latter value depends on the mesh size, which was selected such that the volume of the single element equal to 1 unit of volume. The adopted true stress-strain curve is shown in Fig. 5. The displacement at failure in ABAQUS for each model was calculated based on Eq.15, where l is the element's characteristic length calculated based on the element dimensions (l_1, l_2, l_3) in Eq. 16.

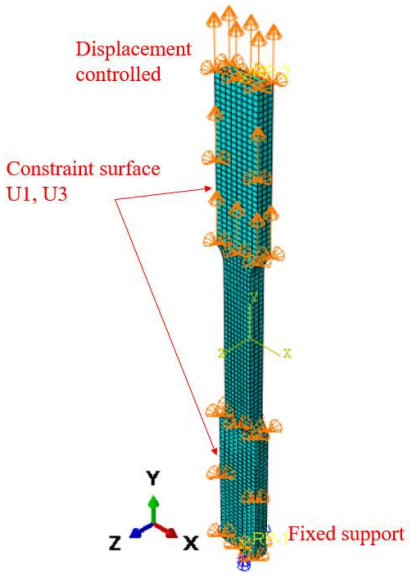

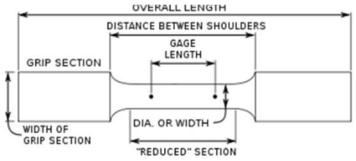

All values in inches	Plate type (1.5 in. wide)	Sheet type (0.5 in. wide)	Sub-size specimen (0.25 in. wide)
Gauge length	8.00±0.01	2.00±0.005	1.000±0.003
Width	1.5 +0.125–0.25	0.500±0.010	0.250±0.005
Thickness	0.188 ≤ T	0.005 ≤ T ≤ 0.75	0.005 ≤ T ≤ 0.25
Fillet radius (min.)	1	0.25	0.25
Overall length (min.)	18	8	4
Length of reduced section (min.)	9	2.25	1.25
Length of grip section (min.)	3	2	1.25
Width of grip section (approx.)	2	0.75	3/8

Figure 4: Numerical model of the coupon and the selected specimen dimensions (ASTM E8, 2010)

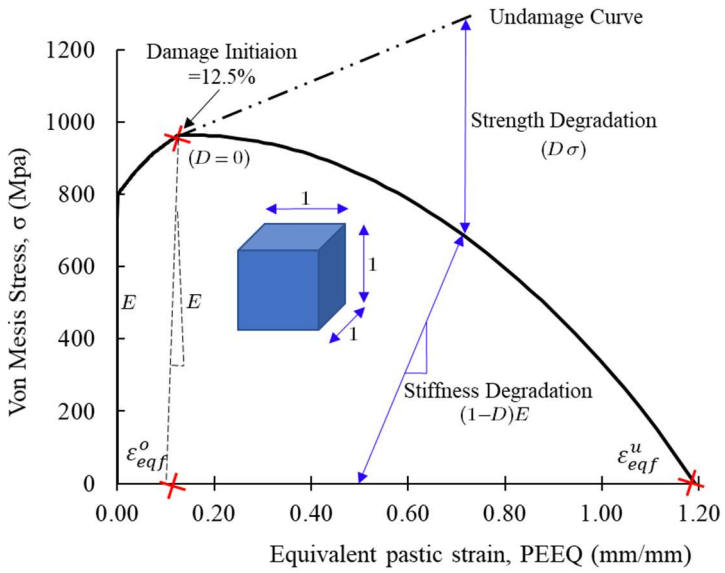

Figure 5: Equivalent stress-strain curve for 800 Mpa steel

$$\varepsilon_{eqf} = \ln(A_R) \tag{14}$$

$$d_f = l^*(\varepsilon^u_{eqf} - \varepsilon^o_{eqf}) \tag{15}$$

$$l = \sqrt[3]{l_1.l_2.l_3} \tag{16}$$

The relationship between the damage initiation and stress triaxiality in the literature (Bao, 2003), (Yu and Jeong, 2010), (Lee, 1993) agrees on dividing the ductility damage mechanism into three regions based on the state of stress as shown in Eq. 17, which describes the relationship between the stress triaxiality and the damage initiation. The coefficient (C) is the equivalent plastic strain for the pure shear state of stress, (n) is the material hardening exponent.

$$\varepsilon_{eqf} = \begin{cases} \infty, & T \le -1/3 \\ C/(1+3T), & -1/3 < T \le 0 \\ C + (\varepsilon^o_{eqf} - C)(T/T_o)^2 & 0 \le T \le T_o \\ \varepsilon^o_{eqf}\dfrac{T_o}{T}, & T \ge T_o \end{cases} \tag{17}$$

$$C = \varepsilon_{eqf}^{o}\left(\frac{\sqrt{3}}{2}\right)^{1/n} \quad (18)$$

Residual Stresses

Different patterns have been proposed for the residual stress distributions and amplitude for the conventional and the high strength steel, even though some researchers have concluded their insignificant effect on the cyclic and monotonic behavior of wid-flange conventional steel column (Elkady and Lignos, 2015). Many experimental studies have demonstrated a comparable residual stress amplitude for conventional and high-strength steel members, which implies the inadequacy of the yield strength-based equations for estimating the residual stresses (Le et al., 2019), (Ban et al., 2008). The stress distribution shown in Fig.6 is recommended by Le et al. (2019) for numerical simulation. The magnitude of the compressive stresses at the web and flanges depends on the cross-section geometry, while the tension stresses at the flange-web junction equal to the steel's yield stress as per Eq. 19 to 21

$$\sigma_{rft} = \sigma_{rwt} = 0.8F_y \quad (19)$$

$$\sigma_{rft} = a_0 + a_1 t_f + a_1 t_f^2 + a_3 / \lambda_f \geq 20MPa \quad (20)$$

$$\sigma_{rwc} = b_0 + b_1 t_w + b_2 t_w^2 + b_3 / \lambda_w \geq 20MPa \quad (21)$$

a_0	a_1	a_2	a_3	b_0	b_1	b_2	b_3
140	−16	0.4	820	115	−10	0	2100

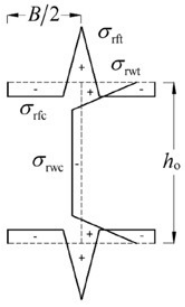

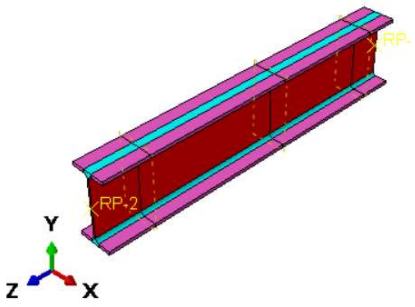

(a) (b) (c)

Figure 6: (a) Coefficient from (Le et al.2019). (b)Residual stress distribution on the cross-section (Le et al.2019). (c) Residual stresses distribution on Abaqus model

Initial Imperfection

The effect of the nonlinear geometry in the FE model requires introducing the shape and the amplitude of the local and global imperfections. The literature does not have a scientific-based method that can predict the initial imperfection of the steel beam. However, it has been customary to use the deformed shape of the first eigenmode for the global imperfection and higher eigenmodes for the local imperfection. The out-of-straightness and out-of-plumpness tolerances in the standard practice code (American Institute of Steel, 2010) are commonly adopted for the imperfection amplitude when there is a lack of data. In other studies, the amplitude of the initial imperfection is selected arbitrarily to match the test results or based on some rules of thumb from the practice. It can be concluded that imposing some local and global imperfections in the steel member is more important than its actual values since it is only needed to trigger the system's instability. The study adopted the shape of the initial imperfection in Fig. 7 based on the buckling analysis of a unit moment applied at the free end.

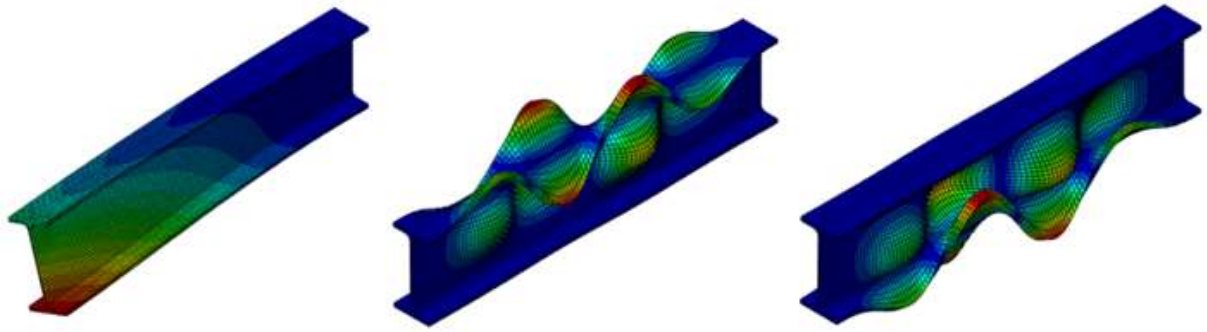

$$Amplitude = \begin{Bmatrix} d/150 & for\ local\ buckling \\ L/1000 & for\ global\ buckling \end{Bmatrix}$$

Figure 7: The selected eigenmodes of the cantilever steel beam to represent the global and local initial imperfection

4. Model Verification

The test results of the high-strength steel beams conducted by Shinohara et al. (2012) and Hai et al. (2019) are used for the purpose of model verifications, as shown in Fig. 8. The numerical simulation demonstrates a reasonable accuracy in terms of the initial stiffness, peak strength, and the area of the hysteresis loops. The stiffness and strength degradation, as well as the point of failure, are reasonably acceptable given the modeling and the test uncertainties. The authors believe that more accurate results can be achieved by considering the missing details of the test setup, such as the actual initial imperfection and the beam-connection interaction, but with a limited influence on the global system behavior in which the beam is a part of it.

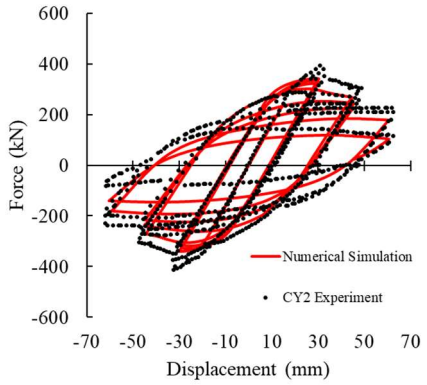
Force (kN)
Displacement (mm)
Numerical Simulation
CY2 Experiment

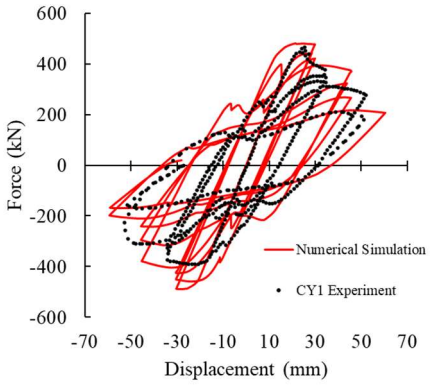
Force (kN)
Displacement (mm)
Numerical Simulation
CY1 Experiment

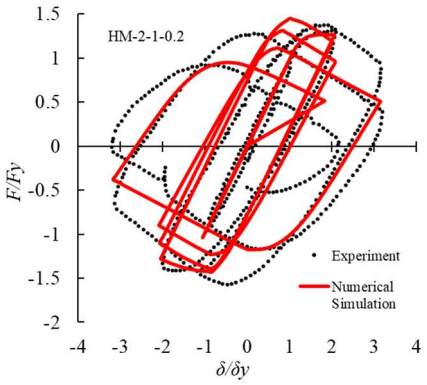
HM-2-1-0.2
F/Fy
δ/δy
Experiment
Numerical Simulation

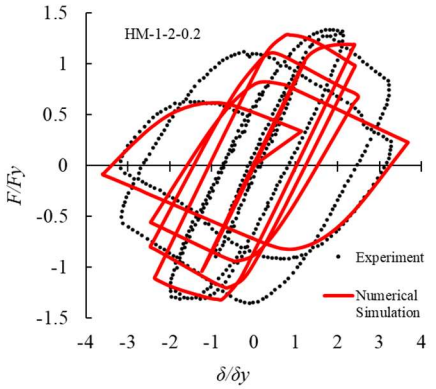
HM-1-2-0.2
F/Fy
δ/δy
Experiment
Numerical Simulation

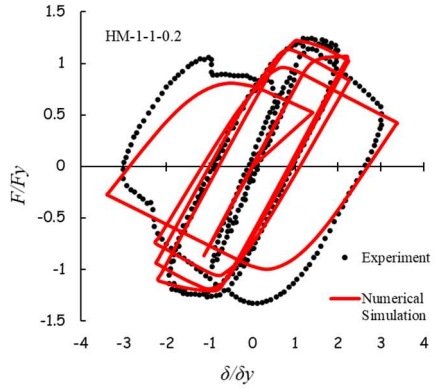
HM-1-1-0.2
F/Fy
δ/δy
Experiment
Numerical Simulation

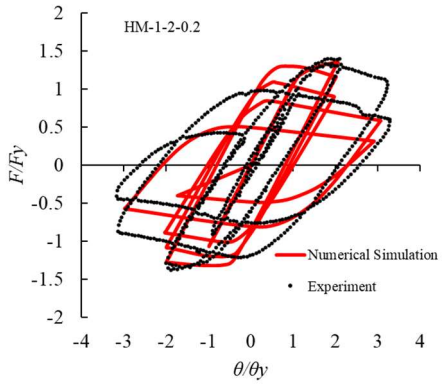
HM-1-2-0.2
F/Fy
θ/θy
Numerical Simulation
Experiment

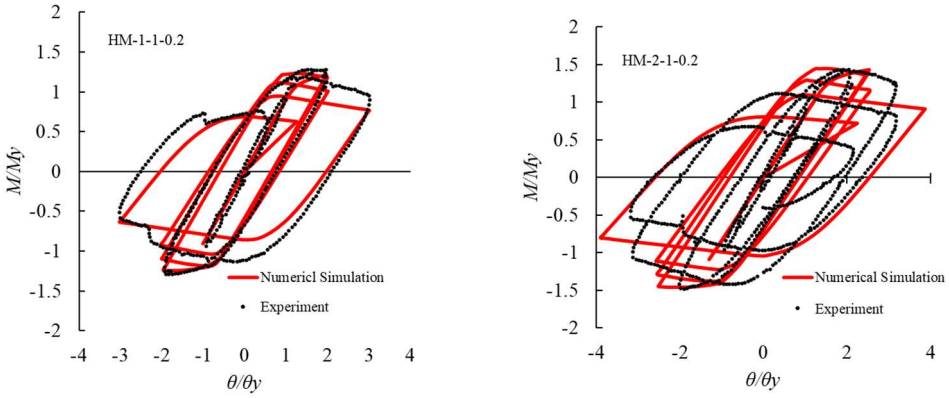

Figure 8: Comparison between prior tests and ABAQUS beam model simulations.

5. Conclusion

This study investigated the monotonic and the cyclic behavior of the high-strength steel beam using a 3D finite element model calibrated based on previous tests. The calibration of the high-strength steel material demonstrated that the equivalent plastic strain at damage initiation for the selected engineering stress-strain curve is 12.5%, and the equivalent plastic strain at failure is about 112.5%-127.5% with linear damage evolution. The analysis results demonstrate that a reasonable geometric imperfection is essential to trigger the system's instability despite the selected shape or amplitude. This paper emphasis the insignificant effect of the residual stresses on the steel beam's hysteretic behavior. The developed numerical models have demonstrated reasonable accuracy in simulating the main cyclic behavior characteristics for different steel beams, such as the elastic stiffness, peak strength, cyclic degradation, and the area of the hysteretic loops.

6. Future work

The establishment of the effective stress-strain curve equations and the fiber-based model is currently under investigation and will be proposed in the next research paper. The assessment of the high-strength steel beam compactness limit and ductility will be investigated in future work.

7. References

ABAQUS-FEA/CAE. (2019). “Dassault Systemes Simulia Corp.” RI, USA.: Dassault Systèmes.

AISC Committee on Specifications, and Ad Hoc Task Group on High Strength Steel. 2019. “High Strength Steel.” Vol. 9.

American Institute of Steel. (2010). “Specification for Structural Steel Buildings.” *American Institute of Steel Construction*, 1–612.

ASTM E8. (2010). “ASTM E8/E8M Standard Test Methods for Tension Testing of Metallic Materials 1.” *Annual Book of ASTM Standards 4*, no. C. https://doi.org/10.1520/E0008.

ATC. 1992. “Guidelines for Cyclic Seismic Testing of Components of Steel Structures.” *ATC-24*.

Ban, Hui Yong, Gang Shi, Yong Jiu Shi, and Yuan Qing Wang. (2008). “Study on the Residual Stress Distribution of Ultra-High-Strength-Steel Welded Sections.” *Gongcheng Lixue/Engineering Mechanics* 25 (SUPPL. 2).

Bao, Yingbin. (2003). “Prediction of Ductile Crack Formation in Uncracked Bodies.” *PhD Thesis*, 252. http://18.7.29.232/handle/1721.1/17634.

Elkady, Ahmed, and Dimitrios G. Lignos. (2015). “Analytical Investigation of the Cyclic Behavior and Plastic Hinge Formation in Deep Wide-Flange Steel Beam-Columns.” *Bulletin of Earthquake Engineering* 13 (4): 1097–1118. https://doi.org/10.1007/s10518-014-9640-y.

Green, Perry S. (2000). “The Inelastic Behavior of High Performance Steel Flexural Members.” *A Dissertation Presented to the Graduate and Research Committee of Lehigh University*. Lehigh University.

Green, Perry S., James M. Ricles, and Richard Sause. (2001). “The Inelastic Behavior of High Performance Steel Flexural Members.” In *Proceedings - Annual Technical Session, Structural Stability Research Council*, 261–90.

Hai, Le Tian, Guo Qiang Li, Yan Bo Wang, Fei Fei Sun, and Hua Jian Jin. (2019). “Experimental Investigation on Cyclic Behavior of Q690D High Strength Steel H-Section Beam-Columns about Strong Axis.” *Engineering Structures* 189 (June): 157–73. https://doi.org/10.1016/j.engstruct.2019.03.060.

Huber, A W. (1958). “Residual Stresses in Wide Flange Beams and Columns . Lehigh University , (July 1956), Revised,” no. July 1956. http://preserve.lehigh.edu/engr-civil-environmental-fritz-lab-.

Jia, Liang Jiu, and Hitoshi Kuwamura. (2014). “Ductile Fracture Simulation of Structural Steels under Monotonic Tension.” *Journal of Structural Engineering (United States)* 140 (5). https://doi.org/10.1061/(ASCE)ST.1943-541X.0000944.

Keeler, Stuart;, and Manachem Kimchi. (2017). “Advanced High-Strength Steels Application Guidelines Version 5.0.” *World AutoSteel.Org*, no. April: 314. http://www.worldautosteel.org/download_files/AHSS Guidelines V6/00_AHSSGuidelines_V6_20170430.pdf.

Le, Tuan, Anna Paradowska, Mark A. Bradford, Xinpei Liu, and Hamid R. Valipour. (2019). “Residual Stresses in Welded High-Strength Steel I-Beams.” *Journal of Constructional Steel Research*, April. https://doi.org/10.1016/j.jcsr.2019.105849.

Lee, Young-Woong. (1993). “Fracture Prediction in Metal Sheets.” *Republic of Korea M.S. in Mechanical Engineering*.

Rice, J. R., and D. M. Tracey. (1969). “On the Ductile Enlargement of Voids in Triaxial Stress Fields*.” *Journal of the Mechanics and Physics of Solids* 17 (3): 201–17. https://doi.org/10.1016/0022-5096(69)90033-7.

Schillo, Nicole, and Markus Feldmann. (2017). “The Rotational Capacity of Beams Made of High-Strength Steel.” *Proceedings of the Institution of Civil Engineers: Structures and Buildings* 170 (9): 641–52. https://doi.org/10.1680/jstbu.16.00119.

Shinohara, Takuma, Ryota Suekuni, and Kikuo Ikarashi. (2012). “Cyclic Behavior of High Strength Steel H-Shaped Beam.” In *Applied Mechanics and Materials*, 174–177:159–65. https://doi.org/10.4028/www.scientific.net/AMM.174-177.159.

Shome, M., and M. Tumuluru. (2015). “Introduction to Welding and Joining of Advanced High-Strength Steels (AHSS).” In *Welding and Joining of Advanced High Strength Steels (AHSS)*, 1–8. Elsevier Inc. https://doi.org/10.1016/B978-0-85709-436-0.00001-1.

Wang, Yan Bo, Guo Qiang Li, Wei Cui, and Su Wen Chen. (2014). “Seismic Behavior of High Strength Steel Welded Beam-Column Members.” *Journal of Constructional Steel Research* 102: 245–55. https://doi.org/10.1016/j.jcsr.2014.07.015.

Yu, H. L., and D. Y. Jeong. (2010). “Application of a Stress Triaxiality Dependent Fracture Criterion in the Finite Element Analysis of Unnotched Charpy Specimens.” *Theoretical and Applied Fracture Mechanics* 54 (1): 54–62. https://doi.org/10.1016/j.tafmec.2010.06.015.